

RESEARCH

Open Access



# Quantitative evaluation of low-frequency oscillations using real-time phase-contrast MRI during drowsiness

Haoze Zhu<sup>1</sup>, Pan Liu<sup>2,3</sup>, Elodie Foster<sup>1</sup>, Ning Jin<sup>4</sup>, Xiaopeng Zhou<sup>5</sup>, Olivier Balédent<sup>2,3</sup> and Qiuting Wen<sup>1,6\*</sup>

## Abstract

**Background** Low-frequency oscillations (LFOs) in the brain are increasingly recognized for their role in driving brain clearance during sleep and drowsiness. However, human studies have largely relied on qualitative assessment. Quantitative assessments of LFO-driven flow dynamics remain limited, and findings across animal and human studies are mixed. Some report that ventricular CSF inflow is dominated by LFO activity, whereas others suggest that cardiac pulsations are the primary driver of CSF motion along its circulation pathways. In this study, we employed real-time phase-contrast (RT-PC) MRI to quantitatively measure blood and cerebrospinal fluid (CSF) flow rates at the cervical level. Our goal was to assess contributions of LFOs across vascular and CSF compartments and to examine their changes between wakefulness and drowsiness.

**Methods** RT-PC MRI was acquired at the cervical (C2/C3) level in thirty-eight healthy participants to measure arterial, venous, and CSF flow rates. Each participant underwent two RT-PC sessions: one with eyes open and another with eyes closed, following a 30-minute in-scanner eyes-closed rest period. Frequency-domain analysis quantified power within LFO, respiratory, and cardiac bands across artery, vein, net arteriovenous flow (A+V), and CSF signals. Time domain analysis was used to calculate arterial-to-venous delays (A-V delay) for each pulsation type.

**Results** Cardiac pulsations dominated the flow rate oscillations, accounting for 95.2%, 85.1%, 81.2%, and 94.2% of the total power in artery, vein, A+V, and CSF, respectively. LFO contributions were lower, accounting for 3.2%, 4.9%, 3.5%, and 0.8%. After 30 min of rest, LFO power increased significantly and consistently in all compartments ( $p < 0.01$ ) but remained a minor component of the overall oscillatory signal. Time domain analysis revealed a longer A-V delay in the LFO band (318 ms) compared to the cardiac band (82 ms), with both delays showing no change after rest ( $p > 0.1$ ).

**Conclusion** Quantitative flow analysis demonstrated that LFOs contributed substantially less to blood and CSF flow oscillations than cardiac pulsations at the cervical level. However, LFO power increased significantly and consistently after rest in blood and CSF, supporting its role as a driver of fluid circulation during drowsiness. Notably, the detection of increased LFO power in arterial blood at the cervical level—upstream of cerebral flow—suggests a potential link to autonomic regulation of vascular tone.

\*Correspondence:

Qiuting Wen  
wenq@iu.edu

Full list of author information is available at the end of the article



© The Author(s) 2025. **Open Access** This article is licensed under a Creative Commons Attribution-NonCommercial-NoDerivatives 4.0 International License, which permits any non-commercial use, sharing, distribution and reproduction in any medium or format, as long as you give appropriate credit to the original author(s) and the source, provide a link to the Creative Commons licence, and indicate if you modified the licensed material. You do not have permission under this licence to share adapted material derived from this article or parts of it. The images or other third party material in this article are included in the article's Creative Commons licence, unless indicated otherwise in a credit line to the material. If material is not included in the article's Creative Commons licence and your intended use is not permitted by statutory regulation or exceeds the permitted use, you will need to obtain permission directly from the copyright holder. To view a copy of this licence, visit <http://creativecommons.org/licenses/by-nc-nd/4.0/>.

**Keywords** Real-time phase contrast MRI, Low-frequency oscillation, Arteriovenous blood, Cerebrospinal fluid, Drowsiness, Wakefulness, Autonomic regulation, Physiology

## Background

CSF plays a vital role in the brain's waste clearance function, yet the physiological drivers of CSF circulation remain incompletely understood [1, 2]. Cardiac pulsations, respiration, and low-frequency oscillations (LFOs) have been proposed as possible forces influencing CSF dynamics [3]. Traditionally, cardiac pulsations have been considered the dominant driver. However, recent modeling studies suggest that cardiac pulsations alone may be insufficient to generate directional CSF flow [4–6]. In contrast, LFOs have gained increasing recognition as an important driver of fluid clearance. In rodent studies, elevated LFOs in vessel wall movements, driven by neurovascular coupling or autonomic activity, have been associated with enhanced CSF waste clearance in the interstitial space during both wakefulness [7–9] and sleep [10, 11]. Human studies using functional magnetic resonance imaging (fMRI) also support the role of LFOs as critical drivers of CSF dynamics, particularly during sleep and drowsiness [12–15].

With the growing interest in LFOs, a deeper understanding of their contribution to blood and CSF flow in awake and drowsy states is needed. Direct and quantitative assessments of LFO-driven flow dynamics remain limited, and existing studies offer mixed findings on the magnitude of LFOs in both vascular and CSF flow. For instance, animal studies measuring vascular diameter have reported strong LFO-related oscillations in pial artery diameter [7, 16, 17]. In contrast, particle-tracking studies that quantify CSF rate in the perivascular space indicate cardiac-dominant CSF flow with minimal LFO influence [18, 19]. In humans, fMRI-based assessments at the fourth ventricle have shown dominant LFO oscillations in CSF inflow dynamics during both wakefulness [20, 21] and sleep [12, 15, 22]. Yet, phase-contrast MRI and dynamic diffusion-weighted studies primarily attribute CSF flow to cardiac pulsations and respiration [23–28, 29]. These discrepancies highlight critical gaps in understanding the relative contributions of LFO, respiration, and cardiac pulsations to blood and CSF flow, as well as how these proportions shift between wakefulness and drowsiness. They also reflect the challenges of interpreting results across various MRI techniques, particularly between quantitative and qualitative flow measurements.

PC-MRI enables the quantitative evaluation of flow dynamics and has yielded significant findings on cardiac-driven CSF flow through cardiac-gated acquisitions [23, 30]. Recent advancements in high-temporal-resolution real-time PC-MRI (RT-PC) have facilitated real-time

monitoring of flow rate, providing key insights into respiration-driven CSF dynamics [24, 31–33]. However, most RT-PC studies use scan durations of less than one minute, limiting the ability to assess the LFO component.

In this study, we leverage high-temporal-resolution RT-PC to continuously monitor blood and CSF flow at the cervical level over an extended period. This approach allows for a quantitative assessment of flow rate oscillations and their contributions from LFO, respiratory, and cardiac pulsations. To study whether these contributions change during drowsiness, we acquired RT-PC scans under two conditions: one during wakefulness with eyes open and one during drowsiness after 30 min of in-scanner eyes-closed rest. We hypothesize that (1) LFOs contribute less to blood and CSF flow rate oscillations than respiration and cardiac pulsations, and (2) LFO contribution increases during drowsiness.

## Methods

### Participants

The current study recruited 40 healthy, neurotypical adults without a history of neurological diseases or cancer. They provided written informed consent in accordance with procedures approved by the Institutional Committee for the Protection of Human Subjects at Indiana University. Two participants were excluded due to poor data quality associated with motion. The final sample included 38 participants (9 males and 29 females) aged  $53.08 \pm 13.12$  years, with an age range of 35–82 years.

### Image acquisition

MRI data were collected using a 3T scanner (MAGNETOM Prisma, Siemens Healthineers, Forchheim, Germany) with a 64-channel head-neck coil at Indiana University. A three-dimensional magnetization-prepared rapid gradient echo (MPRAGE, 1 mm isotropic resolution) sequence was used to localize the cervical level (C2/C3). RT-PC MRI was acquired at the C2/C3 plane to capture arteriovenous and CSF flow. Each participant completed two sessions separated by a 30-minute period of uninterrupted eyes-closed rest to encourage drowsiness. Session 1 was conducted with eyes open. After the 30-minute eyes-closed rest, session 2 was conducted with eyes closed (Figure S1). Each session comprised two RT-PC scans with velocity encoding set to 70 cm/s for arterial and venous flow and 10 cm/s for CSF flow.

The RT-PC sequence utilized an EPI-based multi-shot, Cartesian trajectory with parallel imaging acceleration and shared velocity encoding [34]. By pairing

adjacent frames to form velocity estimates, the shared velocity encoding reduces the number of encodes per sample—achieving effective temporal resolutions of 48 ms for blood flow and 54 ms for CSF. Additional acquisition parameters were as follows: field of view = 240 mm, number of shots per image = 4, voxel size =  $1.1 \times 1.1 \times 10$  mm<sup>3</sup>, flip angle = 10 degrees, 3063 temporal points, and total scan time = 2 min 27s/ 2 min 46s for blood flow and CSF, respectively. Due to the maximum allowable temporal points being limited to 1021 (~ 50 s), the extended scan time was achieved by repeating the ~ 50s sequence three times consecutively, with ~ 3-second gaps between repetitions.

To characterize the drowsiness state during both sessions—defined as a transitional condition between wakefulness and light sleep—Stanford Sleepiness Scale (SSS) was administered immediately after scanning.

Participants rated their perceived drowsiness levels for each session using the 8-point SSS, where 1 indicates wide awake and 8 represents asleep [35, 36]. The SSS is a well-established subjective measure of physiological arousal and has been validated against objective indicators such as EEG and reaction time measures [37–41]. Finger pulse and respiration were monitored using the scanner's built-in finger photoplethysmography and respiration belt. The extracted physiological metrics comprised heart rate, heart rate variability (measured as the standard deviation of the R-R interval).

#### RT-PC preprocessing

A semi-automatic segmentation algorithm was utilized to delineate arteries (internal carotid and vertebral arteries), veins (internal jugular vein), and spinal CSF regions [42] (Fig. 1A). Aliasing and background corrections were

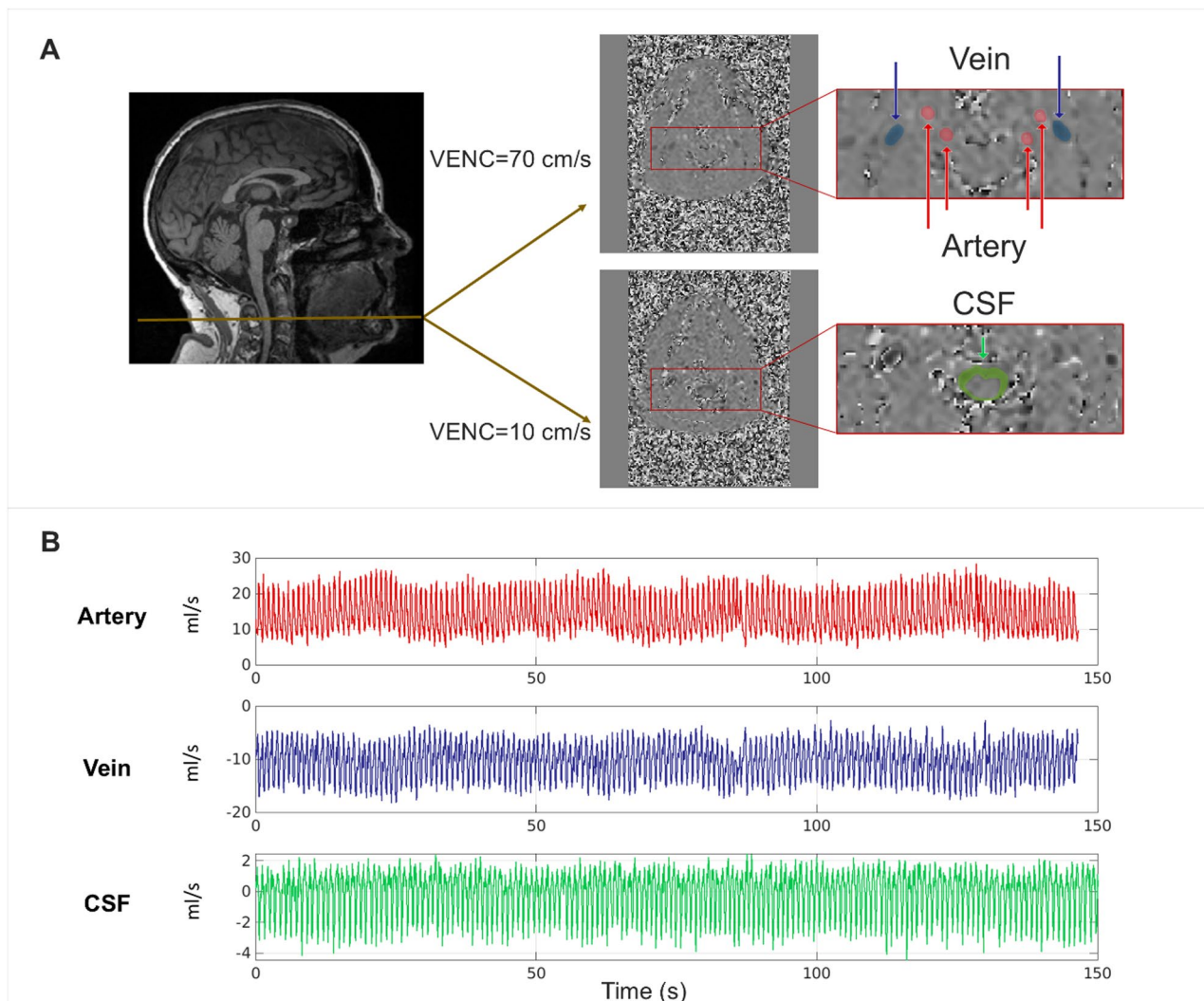


**Fig. 1** Overview of data collection and signal extraction. **A**) Regions of interest (ROIs) for the internal carotid arteries (ICA), vertebral arteries, internal jugular veins (IJV), and CSF in the spinal canal from one subject. The brown plane in the sagittal T1 image marks the C2/C3 level. Two VENCs were set to measure blood flow (VENC = 70 cm/s) and CSF (VENC = 10 cm/s). **B**) Mean RT-PC flow rate waveforms in the artery, vein, and CSF of a representative participant

performed using functions from Flow 2.0 [42]. Aliasing was automatically corrected by detecting aliased voxels exceeding VENC and applying a phase-unwrapping step to recover the true velocity magnitude and sign. Background offsets were removed by estimating a zero-velocity reference from surrounding stationary tissue at each slice and time point and subtracting it from all voxels. Motion-related ROI drift was assessed via frame-by-frame visual inspection of vessel ROIs, and manual adjustments were applied as needed.

Flow rates of arterial, venous, and CSF were computed from phase data by multiplying the mean flow velocity within each ROI by the corresponding ROI area, using a previously validated pipeline [43]. The arterial signal was computed as the average of the bilateral internal carotid arteries and vertebral arteries. The venous signal was derived from the bilateral internal jugular veins. The CSF signal was obtained from the spinal canal. The net blood flow ( $A + V$ ) into the brain was estimated as the sum of arterial inflow (positive, caudal-to-cranial direction) and venous outflow (negative, cranial-to-caudal direction) scaled by a correction factor  $\lambda$ , as used in previous studies [32, 44]. The  $\lambda$  was determined by dividing the mean arterial flow by the mean venous flow, thereby ensuring a near-zero net flow over a cardiac cycle. In principle, the arterial inflow should match the venous outflow over a cardiac cycle. However, measured arterial flow can exceed measured venous flow, because venous anatomy varies substantially across individuals and small, low-velocity venous branches are often not captured at typical PC-MRI spatial resolution and VENC. Applying  $\lambda$  corrects this mismatch and reduces bias in the net-flow estimate.

The forecast package in R was then applied to fill in the 3-second gap between repeated RT-PC sequences [45]. This forecast method utilizes the pattern of the known signal to predict the unknowns and has been widely used to fill in the missing data in a time series [46–50]. The signals before and after the gap filling of a representative participant were shown in Supplementary Figures S2 and S3, demonstrating the robustness of the methods.

#### Frequency- and time-domain analysis

Frequency-domain analyses were performed to quantify oscillation powers in the LFOs, respiration, and cardiac pulsations. The Fast Fourier Transform was applied to transfer the demeaned real-time flow rates to the frequency domain. Power spectral density was used to calculate the band power within the LFOs (0.01–0.1 Hz), respiratory (0.15–0.4 Hz), and cardiac (participant-specific cardiac frequency  $\pm 0.3$  Hz) bands (Fig. 2A). In addition, normalized band power was calculated for each frequency band by dividing its power by the total power of all three bands.

Time-domain analyses were performed to calculate the A-V delay for LFOs, respiratory, and cardiac oscillations. RT-PC signals of arterial and venous flow rates were demeaned and bandpass filtered to extract the signal oscillation in the LFO, respiratory, and cardiac frequencies. For each pulsation type, the time lag and correlation coefficient between the artery and vein signal were acquired by cross-correlation (MATLAB: `xcorr`). In addition, the standard deviation of the temporal signals in LFO, respiratory, and cardiac bands was computed to evaluate signal fluctuation changes between wakefulness and drowsiness states.

#### Statistical analyses

Paired t-tests were used to compare differences between two conditions, such as the power of LFOs versus cardiac pulsations, or between wakefulness and drowsiness. Then the Lilliefors test was used to assess normality. For comparisons that did not meet the normality assumption, the Wilcoxon signed-rank test was applied. All statistical tests were controlled for multiple comparisons using false discovery rate (FDR) correction, with significance defined as  $p < 0.05$  (FDR-corrected).

## Results

### Dominant cardiac and minor LFO oscillations in blood and CSF flow rate

Frequency-domain analysis revealed that cardiac pulsations contributed most prominently to flow rate oscillations across both blood and CSF compartments, whereas LFO contributions were comparatively minor (Fig. 2A–C). Specifically, cardiac pulsations accounted for 95.2%, 85.1%, 81.2%, and 94.2% of the total power in the artery, vein,  $A + V$ , and CSF, respectively. In contrast, LFOs contributed 3.2%, 4.9%, 3.5%, and 0.8% in these compartments (Fig. 2C). Respiration contributions were lower than LFOs in arteries (1.6%), but higher than LFOs in venous and CSF flow (10.0% and 5.0%, respectively). When comparing LFOs across flow compartments, LFO power was significantly lower in CSF compared to vascular compartments (FDR-corrected  $p < 0.001$ , effect size  $d = 0.55, 0.71, \text{ and } 0.64$  for artery, vein, and  $A + V$ , respectively) (Fig. 2D). Detailed statistical results of Fig. 2 are presented in Tables S1 and S2.

### Longer A-V delays in LFOs compared to the cardiac frequency

Among the 38 participants, both LFOs and cardiac signals exhibited consistent A–V delays across individuals, whereas respiratory oscillations did not show a consistent pattern (Fig. 3). The average time lag and correlation coefficient were  $318 \pm 91$  ms and 0.75 for LFOs, and  $82 \pm 44$  ms and 0.95 for the cardiac band. The A–V delay was significantly longer for LFOs compared to the

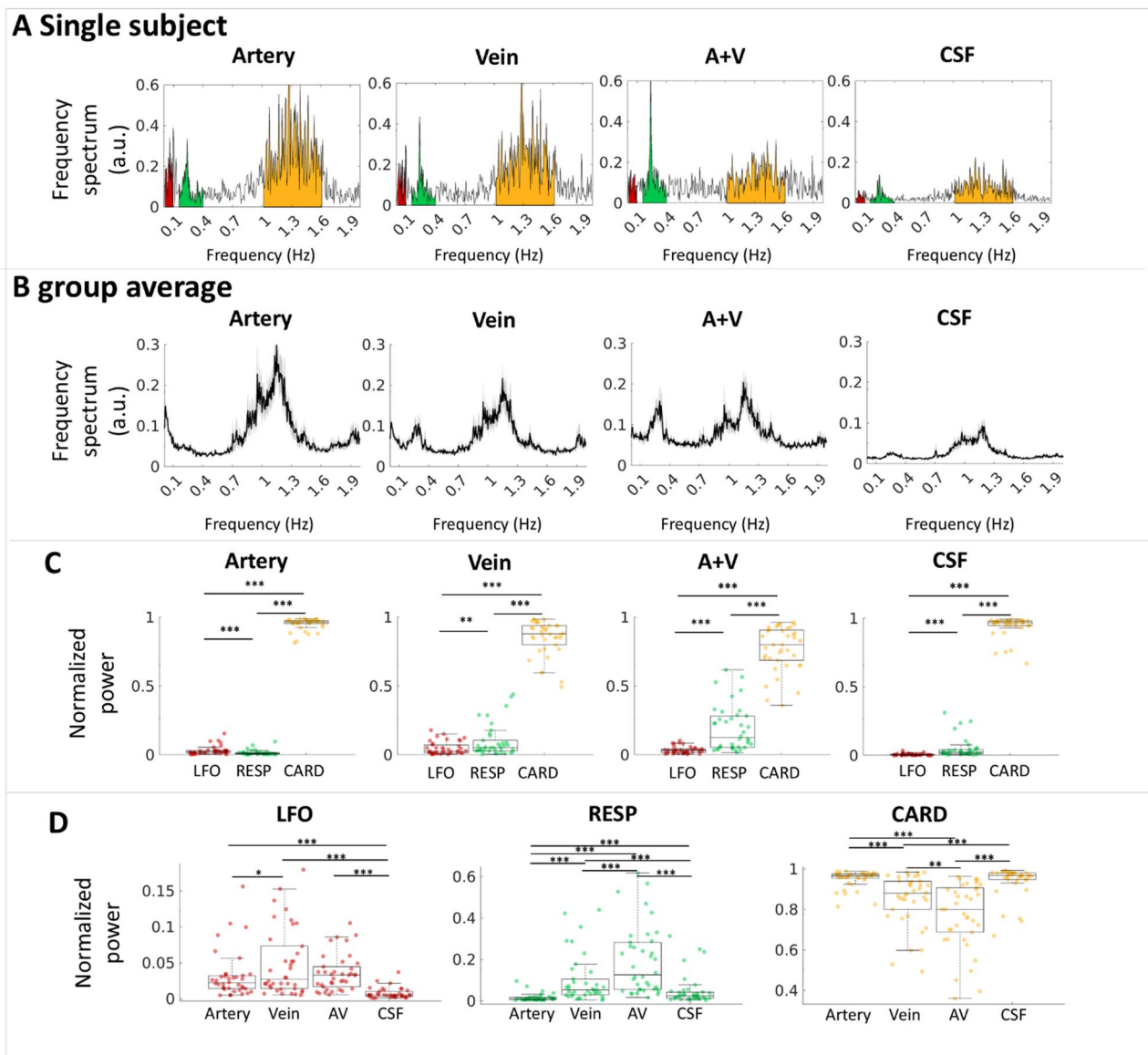


**Fig. 2** Low LFO and high cardiac power in blood and CSF flow during wakefulness. **A**) Frequency spectra from a representative subject during wakefulness showing LFOs (red), respiration (green), and cardiac (yellow) components across different fluid compartments. **B**) Group-averaged frequency spectra ( $N=38$ ); Lines and shaded area indicate mean and standard error. **C**) Comparisons of normalized band power across frequency components grouped by ROIs. **D**) Comparison of normalized band power across ROIs grouped by frequency components. \* $p < 0.05$ , \*\* $p < 0.01$ , \*\*\* $p < 0.001$  using paired t-test with FDR corrections; A + V: sum of arterial inflow and venous outflow (net blood flow into the brain)

cardiac pulsations (Wilcoxon signed-rank test,  $z = 2.94$ , FDR-corrected  $p < 0.01$ ).

#### LFOs increased from wakefulness to drowsiness in all fluid compartments

LFO power increased across all fluid compartments during drowsiness (Fig. 4). Specifically, LFO power was significantly higher after 30-minute rest in arterial ( $d = 2.00$ , FDR  $p < 0.001$ ), venous ( $d = 1.30$ , FDR  $p < 0.01$ ), A + V ( $d = 1.40$ , FDR  $p < 0.01$ ), and CSF flow oscillations ( $d = 1.58$ , FDR  $p < 0.01$ ). In contrast, cardiac power significantly decreased in venous flow ( $d = -1.30$ , FDR  $p < 0.001$ )

and increased in CSF flow ( $d = 0.48$ , FDR  $p = 0.02$ ), and showed no change in arterial flow (Wilcoxon signed-rank,  $p > 0.1$ ). Respiration power did not change in any fluid compartment. Additionally, the increase in LFO power during drowsiness was further confirmed by time-domain analyses, which demonstrated elevated temporal signal variability in the LFO band during drowsiness (Figure S4). A–V delays of LFOs and cardiac bands revealed no significant changes during drowsiness (Wilcoxon signed-rank,  $p > 0.1$ ).

All participants reported increased drowsiness after the 30-minute rest, with the Stanford Sleepiness Scale (SSS)

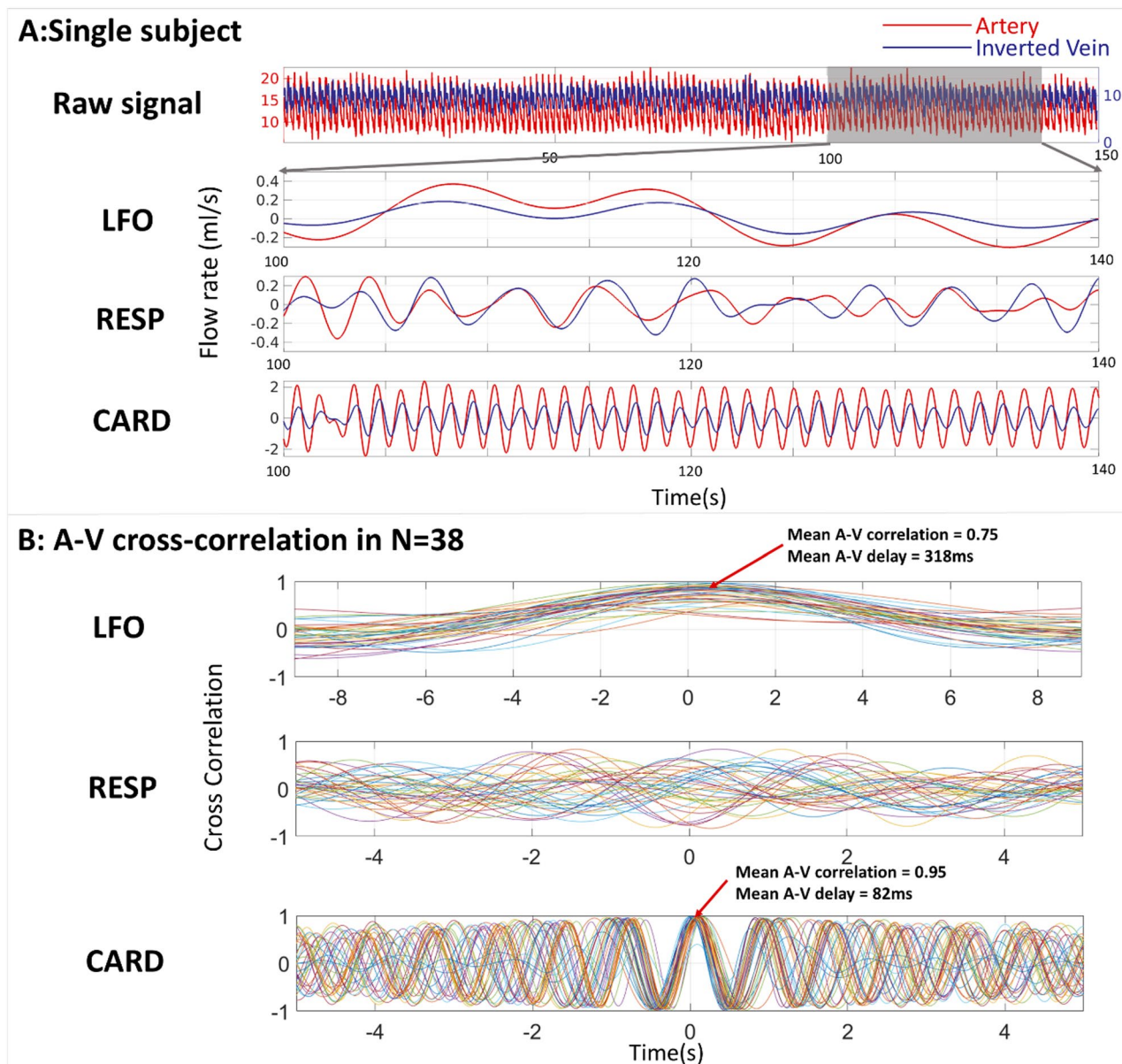


**Fig. 3** A-V delay is longer in LFOs than in cardiac pulsations. **A)** Time-domain flow signals and filtered LFOs, respiratory, and cardiac components from one representative participant. Arterial flow is shown in red, and venous flow is shown in blue. To better visualize the coupling between arterial and venous flow, the venous signal was inverted. **B)** Cross-correlation curves between arterial and venous signals across participants ( $N=38$ ) show a mean A-V delay of 318ms for LFOs, significantly longer than the 82 ms delay for cardiac pulsations (Wilcoxon signed-rank test,  $z=2.94$ , FDR-corrected  $p < 0.01$ ). Each line represents one subject. A-V delay in the respiratory pulsation is inconsistent and does not exhibit a coherent group-level pattern

scores significantly elevated ( $z=5.39$ , FDR  $p < 0.001$ ) (Figure S5). Among the evaluated physiological parameters, heart rate variability demonstrated the most change, with a trending increase approaching significance after FDR correction (Wilcoxon signed-rank  $z=1.84$ , FDR  $p=0.09$ ). No significant association was found between changes in SSS scores and the level of LFO power increase (results not shown).

## Discussion

This study employed RT-PC imaging to quantify the relative contributions of LFOs in the CSF and blood flow during wakefulness and drowsiness. Our findings indicate that LFOs contribute minimally to CSF (~1%) and blood flow (3–5%) rate oscillations, with their influence being significantly smaller than cardiac pulsations (LFOs  $\ll$  cardiac) in both wakefulness and drowsiness. However, after 30 min of eye-closed rest, LFOs exhibited the most significant and consistent increase in both

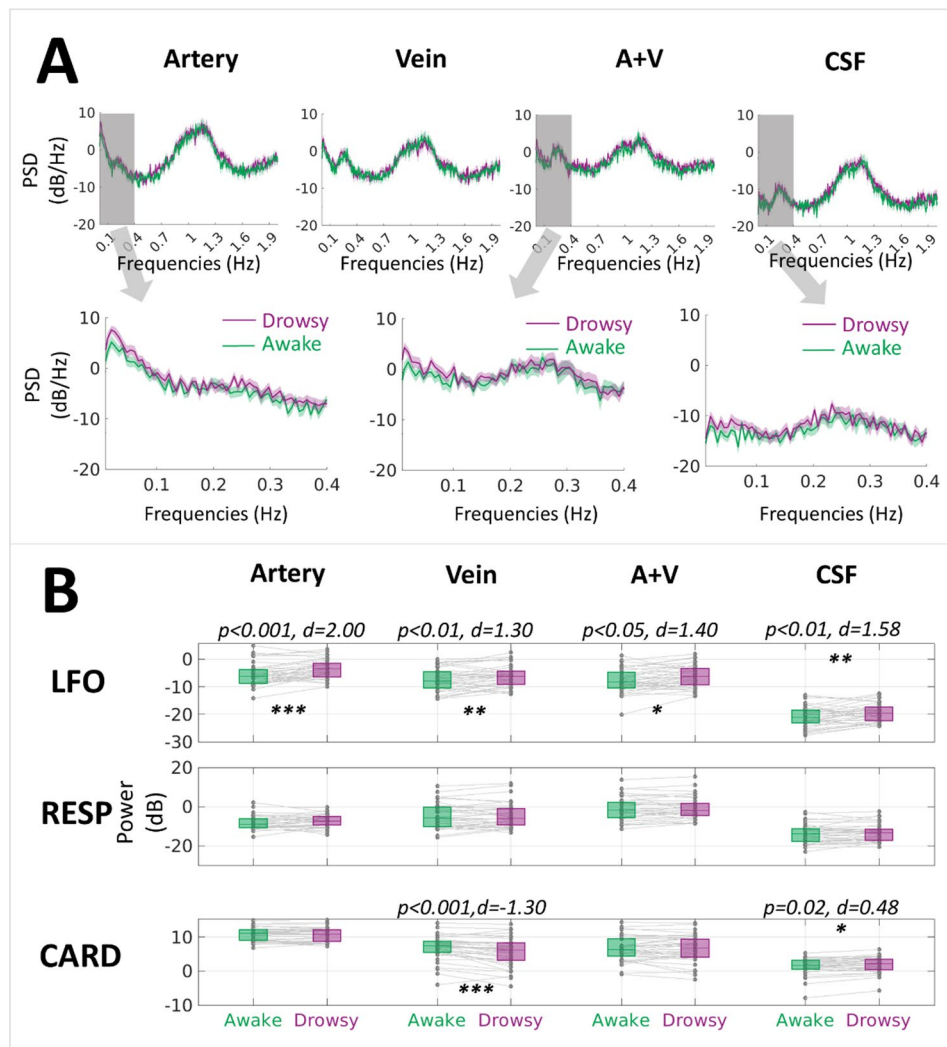


**Fig. 4** Increased LFOs during drowsiness. **A** Comparison of mean power spectrum density (PSD) between wakefulness and drowsiness. The bottom zoomed-in plot (0–0.4 Hz) shows higher LFO power during drowsiness (purple) compared to wakefulness (green). **B** Box plots show increased LFO power during drowsiness across all flow compartments. Cardiac power decreases in the vein and increases in the CSF.  $p < 0.05$ ,  $**p < 0.01$ ,  $***p < 0.001$ ; A+V: sum of arterial inflow and venous outflow.  $d$  = Cohen's  $d$

CSF and blood flows, where respiration and cardiac pulsations showed either no detectable changes or inconsistent trends. Additionally, while cardiac pulsation demonstrated an A–V delay of 82 msec, the A–V delay in the LFOs was notably longer, measuring 318 msec. These results provide quantitative evaluations of LFO and cardiac contributions to fluid dynamics, with their broader implications discussed below.

#### The smaller contribution of LFOs to flow rate oscillations

LFOs are increasingly recognized as key drivers of CSF waste clearance [12, 14, 21]. Our findings indicate that LFOs contribute less than 5% to CSF and blood flow rate oscillations at the cervical level across different drowsiness states, whereas the cardiac (>75%) component plays a more dominant role. While this pattern is consistent

with large-arterial flow behavior in the brain [51], it contrasts with the strong LFOs of CSF dynamics observed at the fourth ventricle using fast fMRI [12, 20]. The discrepancy may arise from the distinct contrast mechanisms of PC MRI and fMRI. PC MRI directly measures flow rate in milliliters per second [52, 53], while fMRI is sensitive to CSF inflow effects [12]. Specifically, when the bottom imaging slice is placed at the fourth ventricle or spinal canal, fMRI signal intensity increases as fresh CSF enters the slice before being exposed to radiofrequency pulses. Thus, voxel intensity reflects CSF volume changes over the repetition time (TR) [54]. Mathematically, volume change represents the integral of flow rate over time, meaning that fMRI acquisition acts as a low-pass filter – amplifying slow oscillations while attenuating faster oscillations such as cardiac and respiratory pulsations. In this

context, LFOs, although subtle in amplitude, persist over extended time and can produce substantial cumulative volume displacements. Therefore, volume-based metrics of LFOs may detect a higher contribution than flow rate metrics. Supporting this, a recent study using simultaneous RT-PC and fMRI acquisitions at the fourth ventricle similarly reported a delay between CSF flow rate and CSF inflow, suggesting that PC-MRI and fMRI capture different aspects of CSF dynamics [55]. Furthermore, when a recent quantitative modeling approach was applied to convert fMRI inflow fluctuations into estimated CSF flow rate, the dominant LFO pattern disappeared, and cardiac pulsations became predominant [56]. Collectively, these findings highlight distinct contrast mechanisms between PC-MRI and fMRI that warrant careful interpretation. Our results reinforce that cardiac pulsation remains the dominant driver of blood and CSF flow rate dynamics at the cervical level.

#### Increased LFOs power from wakefulness to drowsiness

Despite its smaller contribution to flow rate oscillations, LFO power significantly increased in both blood and CSF flow at the cervical level during drowsiness. This aligns with previous reports of elevated LFO power in cerebral hemodynamics and ventricular CSF flow using the fNIRS and fast fMRI [12, 22, 57–61]. Notably, our study observed an increase in arterial LFO power at the cervical level—upstream of cerebral flow—suggesting potential involvement of autonomic regulation.

Previous studies have proposed that the LFO increase during drowsiness may arise from two mechanisms: one involving change in electrocortical activity, where increased delta (0.5–4 Hz) and decreased alpha (8–13 Hz) EEG power promote blood and CSF LFOs through neurovascular coupling [12]; and the other involving autonomic-driven mechanisms, where changes in cerebral vascular tone are mediated by autonomic nervous system activity [15, 62]. Our observation of increased LFO power in cervical arterial blood supports the autonomic mechanism. As vigilance declines, parasympathetic activity (associated with calm and rest) increases, reflected by increased heart rate variability as observed in our participants, which may directly promote systemic low-frequency oscillations throughout the vascular networks [63]. Nevertheless, these two mechanisms are likely interrelated, collectively contributing to the observed increase in LFO power in CSF during drowsiness. Our findings support the potential role of LFOs as a driver of fluid clearance during rest.

#### A-V delay

By simultaneously assessing arterial and venous flow dynamics, we identified a mean A-V delay of 82 ms in the cardiac band and 318 ms in the LFOs band, whereas

respiratory oscillations did not exhibit a reliable delay. The observed 82 ms cardiac-band delay falls within the range reported in prior studies, which documented delays between 43 ms and 171 ms [64–69]. In contrast, the 318 ms A-V delay in the LFOs band was significantly longer than the cardiac-band delay (318 ms vs. 82 ms). This difference reflects the slower propagation velocity of vasomotion-driven waves compared to cardiac pulse waves. A prior human study estimated vasomotion waves propagating along facial blood flow at 3.8 mm/s [70], whereas cardiac pulse waves travel at 4 m/s in the arteries [71]. Notably, the 318 ms A-V delay in the LFOs band was substantially shorter than the few seconds delay previously reported in fMRI studies for the blood transit time from cerebral arteries to veins [72, 73]. This discrepancy reflects differences in the physiological properties captured by fMRI vs. PC-MRI. In fMRI, the observed time lag represents blood transit through the vasculature, encompassing oxygen exchange at the capillary level and subsequent venous drainage, similar to tracking a contrast bolus [74]. In contrast, A-V delay measured in PC-MRI reflects the mechanical propagation of a pressure wave through the intracranial system: arterial volume expansion transiently increases intracranial blood volume, which must be promptly offset by venous outflow to maintain pressure homeostasis, consistent with the Monro-Kellie doctrine. To our knowledge, the 318 ms A-V delay in LFO measured by RT-PC is reported here for the first time. The high cross-correlation between arterial and venous LFO signals ( $r = 0.75$ ) and the delay direction supports the notion that venous LFO pulsations originate from arterial system fluctuations. Moreover, our findings indicate that A-V delays in both cardiac-band and LFO-band remain stable between wakefulness and drowsiness, despite an overall increase in LFO amplitude.

#### Limitations

The study has several limitations. First, blood and CSF flows were acquired separately using two VENC settings, precluding direct analysis of their dynamic interactions. Multi-VENC PC MRI or intermediate-VENC approaches represent promising tools for simultaneous assessment of blood-CSF coupling [75, 76]. Second, the drowsiness level was evaluated by the self-report scores without EEG monitoring, which prevented objective assessment of drowsiness levels. Third, due to sequence limitations, two ~ 3-second gaps occurred during the 3-minute phase-contrast scans. While undesirable, these gaps accounted for less than 4% of the total data and were interpolated using a machine learning–based gap-filling technique to further minimize potential impact on power estimates. Finally, our scan duration yielded a frequency resolution of ~ 0.0067 Hz, limiting precise characterization of

ultra-low components near 0.01 Hz. Longer acquisitions would improve frequency resolution and enable more reliable evaluation of these ultra-low oscillations.

## Conclusions

By quantitatively evaluating LFOs, respiratory, and cardiac oscillations in CSF and blood flow, our study demonstrated that LFOs contributed little to flow rate oscillations at rest, with cardiac pulsation being the dominant driver. However, LFOs increased most significantly and consistently during drowsiness across all fluid compartments, suggesting a potential role in driving CSF circulation. Notably, the detection of increased LFO power in arterial blood at the cervical level—upstream of cerebral flow—suggests a potential relationship to the autonomic regulation of vascular tone.

## Abbreviations

A+V	Net arteriovenous flow
A-V	Arterial-to-venous
CARD	Cardiac
CSF	Cerebrospinal fluid
FDR	False discovery rate
fMRI	functional MRI
LFO	Low frequency oscillation
RESP	Respiratory
ROI	Region of interest
RT-PC	Real-time phase-contrast
TR	Repetition time

## Supplementary Information

The online version contains supplementary material available at <https://doi.org/10.1186/s12987-025-00741-x>.

Supplementary Material 1

## Acknowledgements

The authors thank Adam M. Wright, Jianing Zhang, Tianyin Xu, and Vidhya Vijayakrishnan Nair for the discussion and advice on the research.

## Author contributions

HZ performed data analysis. PL, XZ, OB, and QW contributed to image processing. EF contributed to data collection. QW conceptualized and designed the study. NJ provided consultation on the imaging sequence. HZ, PL, and QW interpreted the results. HZ and QW drafted the manuscript. PL, XZ, and OB edited the manuscript.

## Funding

This research was supported by the National Institutes of Health under grant number RF1 AG083762.

## Data availability

The data are available upon reasonable request.

## Declarations

### Ethics approval and consent to participate

All participants provided written informed consent according to procedures approved by the Institutional Committee for the Protection of Human Participants at Indiana University.

### Consent for publication

Not applicable.

## Competing interests

The authors declare no competing interests.

## Author details

<sup>1</sup>Department of Radiology and Imaging Sciences, Indiana University School of Medicine, Indianapolis, IN, USA

<sup>2</sup>CHIMRE UR 7516, Jules Verne University of Picardy, Amiens 80000, France

<sup>3</sup>Medical Image Processing Department, CHU Amiens-Picardy University Hospital, Amiens 80000, France

<sup>4</sup>MR R&D Collaborations, Siemens Medical Solution USA, Inc., Malvern, PA, USA

<sup>5</sup>School of Health Sciences, Purdue University, West Lafayette, IN, USA

<sup>6</sup>Weldon School of Biomedical Engineering Department, Purdue University, West Lafayette, IN, USA

Received: 22 May 2025 / Accepted: 19 November 2025

Published online: 08 December 2025

## References

1. Iliff JJ, et al. A paravascular pathway facilitates CSF flow through the brain parenchyma and the clearance of interstitial solutes, including amyloid  $\beta$ . *Sci Trans Med*. 2012; 4(147):147ra111.
2. Bohr T, et al. The glymphatic system: current understanding and modeling. *iScience*. 2022;25(9).
3. Rasmussen MK, Mestre H, Nedergaard M. Fluid transport in the brain. *Physiol Rev*. 2022;102(2):1025–151.
4. Asgari M, De D, Zélicourt, Kurtcuoglu V. Glymphatic solute transport does not require bulk flow. *Sci Rep*. 2016;6(1):38635.
5. Diem AK, et al. Arterial pulsations cannot drive intramural periarterial drainage: significance for A  $\beta$  drainage. *Front NeuroSci*. 2017;11:475.
6. Kedarasetti RT, Drew PJ, Costanzo F. Arterial pulsations drive oscillatory flow of CSF but not directional pumping. *Sci Rep*. 2020;10(1):10102.
7. Holstein-Rønso S, et al. Glymphatic influx and clearance are accelerated by neurovascular coupling. *Nat Neurosci*. 2023;26(6):1042–53.
8. Murdock MH, et al. Multisensory gamma stimulation promotes glymphatic clearance of amyloid. *Nature*. 2024;627(8002):149–56.
9. van Veluw SJ, et al. Vasomotion as a driving force for paravascular clearance in the awake mouse brain. *Neuron*. 2020;105(3):549–61. e5.
10. Jiang-Xie L-F, et al. Neuronal dynamics direct cerebrospinal fluid perfusion and brain clearance. *Nature*. 2024;627(8002):157–64.
11. Hauglund NL, et al. Norepinephrine-mediated slow vasomotion drives glymphatic clearance during sleep. *Cell*. 2025;188(3):606–22. e17.
12. Fultz NE, et al. Coupled electrophysiological, hemodynamic, and cerebrospinal fluid oscillations in human sleep. *Science*. 2019;366(6465):628–31.
13. Helakari H, et al. Effect of sleep deprivation and NREM sleep stage on physiological brain pulsations. *Front NeuroSci*. 2023;17:1275184.
14. Helakari H, et al. Human NREM sleep promotes brain-wide vasomotor and respiratory pulsations. *J Neurosci*. 2022;42(12):2503–15.
15. Picchioni D, et al. Autonomic arousals contribute to brain fluid pulsations during sleep. *NeuroImage*. 2022;249:118888.
16. Bojarskaite L, et al. Sleep cycle-dependent vascular dynamics in male mice and the predicted effects on perivascular cerebrospinal fluid flow and solute transport. *Nat Commun*. 2023;14:953.
17. Munting LP, et al. Spontaneous vasomotion propagates along Pial arterioles in the awake mouse brain like stimulus-evoked vascular reactivity. *J Cereb Blood Flow Metabolism*. 2023;43(10):1752–63.
18. Bedussi B, et al. Paravascular channels, cisterns, and the subarachnoid space in the rat brain: a single compartment with Preferential pathways. *J Cereb Blood Flow Metabolism*. 2017;37(4):1374–85.
19. Mestre H, et al. Flow of cerebrospinal fluid is driven by arterial pulsations and is reduced in hypertension. *Nat Commun*. 2018;9(1):4878.
20. Yang H-C, et al. Coupling between cerebrovascular oscillations and CSF flow fluctuations during wakefulness: an fMRI study. *J Cereb Blood Flow Metabolism*. 2022;42(6):1091–103.
21. Nair VV, et al. Human CSF movement influenced by vascular low frequency oscillations and respiration. 2022.
22. Nair VV, et al. Neurofluid coupling during sleep and wake States. *Sleep Med*. 2023;110:44–53.

23. Rivera-Rivera LA, et al. Four-dimensional flow MRI for quantitative assessment of cerebrospinal fluid dynamics: status and opportunities. *NMR Biomed*. 2024;37(7):e5082.
24. Burman R, Alperin N. CSF-to-blood toxins clearance is modulated by breathing through cranio–spinal CSF Oscillation. *J Sleep Res*. 2024;33(1):e14029.
25. Dreha-Kulaczewski S, et al. Inspiration is the major regulator of human CSF flow. *J Neurosci*. 2015;35(6):2485–91.
26. Wen Q, et al. Assessing pulsatile waveforms of paravascular cerebrospinal fluid dynamics using dynamic diffusion-weighted imaging (dDWI). *NeuroImage*. 2022;260:119464.
27. Wen Q, et al. Dynamic diffusion-weighted imaging of intracranial cardiac impulse propagation along arteries to arterioles in the aging brain. *J Cereb Blood Flow Metab*. 2025;0271678X251320902.
28. Zhang J, et al. Respiration is a driver for parenchyma hydrodynamics: insights from dynamic DWI. In: *Proceedings of the International Society for Magnetic Resonance in Medicine*. Hawaii; 2025.
29. Wright A.M., Wu, YC., Yang, HC. et al. Coupled pulsatile vascular and paravascular fluid dynamics in the human brain. *Fluids Barriers CNS* 21, 71 (2024). <https://doi.org/10.1186/s12987-024-00572-2>
30. Alperin N, et al. Hemodynamically independent analysis of cerebrospinal fluid and brain motion observed with dynamic phase contrast MRI. *Magn Reson Med*. 1996;35(5):741–54.
31. Liu P, Fall S, Balédent O. Use of real-time phase-contrast MRI to quantify the effect of spontaneous breathing on the cerebral arteries. *Neuroimage*. 2022;258:119361.
32. Liu P, et al. Cardiac and respiratory activities induce Temporal changes in cerebral blood volume, balanced by a mirror CSF volume displacement in the spinal Canal. *NeuroImage*. 2025;305:120988.
33. Chen L, et al. Dynamics of respiratory and cardiac CSF motion revealed with real-time simultaneous multi-slice EPI velocity phase contrast imaging. *NeuroImage*. 2015;122:281–7.
34. Lin HY, et al. Shared velocity encoding: a method to improve the Temporal resolution of phase-contrast velocity measurements. *Magn Reson Med*. 2012;68(3):703–10.
35. Shahid A, et al. Stanford sleepiness scale (SSS), in STOP, THAT and one hundred other sleep scales. Springer; 2011. pp. 369–70.
36. Hoddes E, Zarcone V, Dement W. Development and use of Stanford Sleepiness Scale (SSS). *Psychophysiology*. 1972.
37. Maclean AW, et al. Psychometric evaluation of the Stanford sleepiness scale. *J Sleep Res*. 1992;1(1):35–9.
38. Shahid A, et al. STOP, THAT and one hundred other sleep scales. 2012.
39. Chia C-H, et al. Cortical excitability signatures for the degree of sleepiness in human. *Elife*. 2021;10:e65099.
40. Wilhelm B, et al. Pupillographic assessment of sleepiness in sleep-deprived healthy subjects. *Sleep*. 1998;21(3):258–65.
41. Regen F, Dorn H, Danker-Hopfe H. Association between pupillary unrest index and waking electroencephalogram activity in sleep-deprived healthy adults. *Sleep Med*. 2013;14(9):902–12.
42. Liu P, Fall S, Balédent O. Flow 2.0—a flexible, scalable, cross-platform post-processing software for realtime phase contrast sequences. *arXiv preprint arXiv:2207.2022*;12712.
43. Liu P, et al. Validating the accuracy of real-time phase-contrast MRI and quantifying the effects of free breathing on cerebrospinal fluid dynamics. *Fluids Barriers CNS*. 2024;21:25. 1.
44. El Sankari S, et al. Cerebrospinal fluid and blood flow in mild cognitive impairment and Alzheimer’s disease: a differential diagnosis from idiopathic normal pressure hydrocephalus. *Fluids Barriers CNS*. 2011;8:12
45. Hyndman RJ, Khandakar Y. Automatic time series forecasting: the forecast package for R. *J Stat Softw*. 2008;27:1–22.
46. Niako N, et al. Effects of missing data imputation methods on univariate blood pressure time series data analysis and forecasting with ARIMA and LSTM. *BMC Med Res Methodol*. 2024;24(1):320.
47. Pham H-T, et al. Handling missing data in COVID-19 incidence estimation: secondary data analysis. *JMIR Public Health Surveillance*. 2024;10:e53719.
48. Afrifa-Yamoah E, et al. Missing data imputation of high-resolution Temporal climate time series data. *Meteorol Appl*. 2020;27(1):e1873.
49. Benavides IF, et al. Assessing methods for multiple imputation of systematic missing data in marine fisheries time series with a new validation algorithm. *Aquaculture Fisheries*. 2023;8(5):587–99.
50. Bokde N, et al. A novel imputation methodology for time series based on pattern sequence forecasting. *Pattern Recognit Lett*. 2018;116:88–96.
51. Wright AM, Xu T, Tong Y, Wen Q. HyPER: Region-specific hypersampling of fMRI to resolve low-frequency, respiratory, and cardiac pulsations, revealing age-related differences. *Neuroimage*. 2025;321:121502. <https://doi.org/10.1016/j.neuroimage.2025.121502>. Epub 2025 Oct 1. PMID: 41043798.
52. Wymer DT, et al. Phase-contrast MRI: physics, techniques, and clinical applications. *Radiographics*. 2020;40(1):122–40.
53. Williamson NH, et al. Limits to flow detection in phase contrast MRI. *J Magn Reson Open*. 2020;2:100004.
54. Ashenagar B, Gomez DE, Lewis LD. Modeling dynamic inflow effects in fMRI to quantify cerebrospinal fluid flow. *Imaging Neurosci*. 2025;3:pIMAGa9.
55. Roefs EC, et al. BOLD-CSF dynamics assessed using real-time phase contrast CSF flow interleaved with cortical BOLD MRI. *Fluids Barriers CNS*. 2024;21:p107.
56. Söderström P, et al. fMRI-based CSF flow quantification identifies cardiac pulsatility as the dominant driver over respiratory and slow vasomotion cycles. *bioRxiv*. 2025;2025.06.10.658005.
57. Chen Y, et al. Amplitude of fNIRS resting-state global signal is related to EEG vigilance measures: A simultaneous fNIRS and EEG study. *Front Neurosci*. 2020;14:560878.
58. Gaez II, et al. Drowsiness increases slow oscillations in rs-fMRI signal before sleep onset. In: *OHBM 2024 – The Annual Meeting of the Organization for Human Brain Mapping*. 2024.
59. Tuunanen J, et al. Cardiovascular and vasomotor pulsations in the brain and periphery during awake and NREM sleep in a multimodal fMRI study. *Front NeuroSci*. 2024;18:1457732.
60. Wong CW, et al. The amplitude of the resting-state fMRI global signal is related to EEG vigilance measures. *NeuroImage*. 2013;83:983–90.
61. Nair VV, et al. Effect of brief rest on hemodynamics and CSF oscillations across age. *Neuroimage*. 2025;121531.
62. Gold BP, et al. Functional MRI signals exhibit stronger covariation with peripheral autonomic measures as vigilance decreases. *Imaging Neurosci*. 2024;2:1–25.
63. Tong Y, Hocke LM, Frederick BB. Low frequency systemic hemodynamic noise in resting state BOLD fMRI: characteristics, causes, implications, mitigation strategies, and applications. *Front NeuroSci*. 2019;13:787.
64. Stoquart-ElSankari S, et al. A phase-contrast MRI study of physiologic cerebral venous flow. *J Cereb Blood Flow Metabolism*. 2009;29(6):1208–15.
65. Feng J, et al. Phase-contrast MRI indices can reflect intracranial compliance deterioration induced by intra-abdominal/thoracic hypertension. 2021.
66. Bateman G. Pulse-wave encephalopathy: a comparative study of the hydrodynamics of leukoaraiosis and normal-pressure hydrocephalus. *Neuroradiology*. 2002;44:740–8.
67. Rivera-Rivera LA, et al. Changes in intracranial venous blood flow and pulsatility in alzheimer’s disease: A 4D flow MRI study. *J Cereb Blood Flow Metabolism*. 2017;37(6):2149–58.
68. Bhadelia R, et al. Cerebrospinal fluid pulsation amplitude and its quantitative relationship to cerebral blood flow pulsations: a phase-contrast MR flow imaging study. *Neuroradiology*. 1997;39:258–64.
69. Wright AM, Xu T, Koo J, Zhao Y, Tong Y, Wen Q. An fMRI approach to assess intracranial arterial-to-venous cardiac pulse delay in aging. *ImagingNeurosci(Camp)*. 2025;3:IMAG.a.969. <https://doi.org/10.1162/IMA.G.a.969>. PMID: 41178936;PMCID: PMC12576844.
70. Yoshida K, Nishidate I. Phase velocity of facial blood volume Oscillation at a frequency of 0.1 Hz. *Front Physiol*. 2021;12:627354.
71. Obeid H, et al. Radial-digital pulse wave velocity: a noninvasive method for assessing stiffness of small conduit arteries. *Am J Physiol Heart Circ Physiol*. 2021;320(4):H1361–9.
72. Fitzgerald B, et al. Using carpet plots to analyze transit times of low frequency oscillations in resting state fMRI. *Sci Rep*. 2021;11(1):7011.
73. Yao J, et al. Cerebral circulation time derived from fMRI signals in large blood vessels. *J Magn Reson Imaging*. 2019;50(5):1504–13.
74. Tong Y, Frederick Bd. Time lag dependent multimodal processing of concurrent fMRI and near-infrared spectroscopy (NIRS) data suggests a global circulatory origin for low-frequency Oscillation signals in human brain. *NeuroImage*. 2010;53(2):553–64.

75. Rivera-Rivera LA, et al. Simultaneous and synchronous characterization of blood and CSF flow dynamics using multiple Venc PC MRI. *Imaging Neurosci.* 2025;3:imaga00521.
76. Liu P, et al. Synchronous assessment of CSF and cerebral arteriovenous flow interactions across ultra-low, low, respiratory, and cardiac frequencies using real-time phase-contrast MRI. *Neuroimage.* 2025;121490.

**Publisher's note**

Springer Nature remains neutral with regard to jurisdictional claims in published maps and institutional affiliations.